

## System model development and numerical simulation of low-head pumped hydro storage

Hoffstaedt, J. P.; Jarquín-Laguna, A.; Fahlbeck, J.; Nilsson, H.

**DOI**

[10.1201/9781003360773-85](https://doi.org/10.1201/9781003360773-85)

**Publication date**

2023

**Document Version**

Final published version

**Published in**

Trends in Renewable Energies Offshore

**Citation (APA)**

Hoffstaedt, J. P., Jarquín-Laguna, A., Fahlbeck, J., & Nilsson, H. (2023). System model development and numerical simulation of low-head pumped hydro storage. In C. G. Soares (Ed.), *Trends in Renewable Energies Offshore : Proceedings of the 5th International Conference on Renewable Energies Offshore, RENEW 2022* (pp. 757-763). CRC Press / Balkema - Taylor & Francis Group.  
<https://doi.org/10.1201/9781003360773-85>

**Important note**

To cite this publication, please use the final published version (if applicable).  
Please check the document version above.

**Copyright**

Other than for strictly personal use, it is not permitted to download, forward or distribute the text or part of it, without the consent of the author(s) and/or copyright holder(s), unless the work is under an open content license such as Creative Commons.

**Takedown policy**

Please contact us and provide details if you believe this document breaches copyrights.  
We will remove access to the work immediately and investigate your claim.

***Green Open Access added to TU Delft Institutional Repository***

***'You share, we take care!' - Taverne project***

**<https://www.openaccess.nl/en/you-share-we-take-care>**

Otherwise as indicated in the copyright section: the publisher is the copyright holder of this work and the author uses the Dutch legislation to make this work public.

# System model development and numerical simulation of low-head pumped hydro storage

J.P. Hoffstaedt & A.J. Laguna

*Department of Maritime and Transport Technology, Delft University of Technology, Delft, the Netherlands*

J.Fahlbeck & H. Nilsson

*Department of Mechanics and Maritime Sciences, Division of Fluid Dynamics, Chalmers University of Technology, Gothenburg, Sweden*

**ABSTRACT:** To tackle the growing demand for grid-scale energy storage, the ALPHEUS project proposes a novel low-head pumped hydro storage system aimed for coastal application in countries where the topography does not allow for traditional high-head storage. This system consists of a reversible pump-turbine technology with two contra-rotating runners coupled to their respective axial-flux motor-generators as well as a dedicated control, optimising for energy balancing and the provision of ancillary services. To better understand the integration and dynamic interaction of the individual components of the plant and to allow for the simulation of a wide variety of operating conditions and scenarios, this research aims at developing a system model coupling the hydraulic, mechanical and electrical components. Numerical results are compared and verified based on CFD simulations. While some inaccuracies have to be expected, the comparison shows an overall good match with only minor deviations in dynamic behaviour and steady state results.

## 1 INTRODUCTION

With electricity generation being one of the major contributors to the emission of greenhouse gases, countries worldwide are rapidly increasing their share of renewable electricity sources. Depending on the region, solar PV and wind turbines are considered the preferred solution to achieve this aim. Such typically inverter coupled renewable generators introduce intermittency and a reduction in spinning reserves to the electrical grids designed for centralised power plants. To balance the increasing mismatch between demand and supply as well as to provide crucial ancillary services (AS) to stabilise the grid, large-scale energy storage is required.

While pumped hydro storage (PHS) is responsible for the overwhelming majority of energy storage today (REN21 2021), it is traditionally applied in scenarios with high-head differences between the upper and lower reservoir. To enable the technology for usage in regions without sufficient elevation changes, the ALPHEUS project proposes a novel system aimed at low- and ultra low-head (2 - 20 m) scenarios. For such a system it has been proposed that axial-flow reversible pump-turbines (RPT) coupled to axial-flux permanent magnet synchronous machines utilising variable speed drives is one of the most promising

solutions (Hoffstaedt et al. 2022). Additionally, utilising two counter-rotating opposed to a single runner bears the potential to increase efficiency, operating range and reduce the overall size of the pump-turbine (Qudaih et al. 2020).

Aimed at coastal applications, the proposed system can utilise the sea as the upper reservoir with the lower reservoir being separated by a dam. The prototype developed as part of the project uses two runners with a diameter of 6 m each coupled to their individual motor-generator placed in a hub adjacent to the RPT. With a design power rating of 10 MW for each pump-turbines set, multiple sets can be utilised to reach the desired capacity. The lower reservoir is scaled to fulfill the required storage in the timescale of hours to days.

To maximise the potential of a low-head PHS plant contributing to grid stability through energy balancing and AS, reduced switching times between pump and turbine mode and rapid power ramp rates are desired. The transient behaviour of the proposed low-head PHS plant is, however, not yet well understood. To investigate its dynamic behaviour as well as the interaction and influence of the individual components, experiments and numerical simulations are conducted within the ALPHEUS project. Experiments and CFD simulations provide high accuracy results but are

also time and resource intensive and hence limit the amount of scenarios that can be tested. The goal of this research is to develop a comprehensive system model covering the more relevant dynamics of the proposed low-head PHS system while significantly reducing computational resources required.

Despite existing modelling approaches for hydropower and PHS, there is a lack of research on models tailored to low-head scenarios, utilising variable speed operation and integrating two individual runners. Coupling individual components such as the conduit, drivetrain and control into a system model further allows for the investigation of the dynamic interaction of various components. The choice of modelling approaches for these components is determined by weighing up accuracy and performance requirements. Here, the characteristics of the proposed system should be considered. An example for this would be the shift towards lower heads resulting in higher mass flow rates for the same desired power. This shift means inertial effects are more important during sudden changes to the flow rate potentially leading to a higher risk of high amplitude pressure waves commonly known water hammer effects.

This paper presents the system model developed before applying it to a model-scale version of the system proposed by ALPHEUS to be used for a later experimental validation of the project. The results are compared to CFD simulations done by Fahlbeck et al. (2022b). For this, two cases are evaluated. A start-up sequence and rapid change of operating points.

## 2 SYSTEM MODEL OF LOW-HEAD PUMPED HYDRO STORAGE

### 2.1 Flow model inside the conduit

Several approaches exist to model the conduit of PHS plants depending on the required accuracy and computational performance. Approaches that neglect compressibility of the fluid and elasticity of the conduit are computationally efficient and can cover the basic dynamics of the system. However, if transients are to be investigated these effects have to be considered (Mohanpurkar et al. 2018). Hence, for this model a one-dimensional compressible flow approach is chosen. These coupled partial differential equations shown in Eq. 1 and Eq. 2 (Stecki and Davis 1986) are based on the fundamental equations of conservation of mass and momentum and are also known as water hammer equations.

$$\frac{\partial H}{\partial t} = -U \frac{\partial H}{\partial x} - \frac{a^2}{g} \frac{\partial U}{\partial x} \quad (1)$$

$$\frac{\partial U}{\partial t} = -U \frac{\partial U}{\partial x} - g \frac{\partial H}{\partial x} - S \quad (2)$$

Here  $H$  is the pressure head,  $U$  the fluid velocity,  $a$  the effective pressure wave velocity in the fluid,  $g$

the gravitational acceleration,  $D$  the conduit diameter and  $S$  the friction losses. If the pressure wave velocity in the pipe is much greater than the fluid velocity and the conduit is cylindrical the convective terms given by  $-U \frac{\partial H}{\partial x}$  and  $-U \frac{\partial U}{\partial x}$  can be neglected (Sharma and Kumar 2014). The speed of pressure waves within the conduit depends on the stiffness of the pipe and the compressibility of the liquid (Ghidaoui 2004). In a stiff conduit of a hydroelectric power plant with potentially some gas bubbles forming due to cavitation caused by pressure transients, the pressure wave velocity can be assumed to be between 1000 and 1480 m/s. In the scenario considered, the fluid velocity will not exceed 6 m/s.

Conical pipe sections such as draft tubes can be modelled using an approximation based on equivalent pipe elements. Alternatively, changes to the velocity head have to be considered in the momentum equation and the continuity equation is extended as shown in Eq. 3 (Adamkowski 2003) with  $A$  being the cross-sectional area of the conduit. Additional expansion and contraction losses should be considered.

$$\frac{\partial H}{\partial t} = -\frac{a^2}{g} \frac{\partial U}{\partial x} - \frac{a^2}{g} U \frac{\partial \ln A}{\partial x} \quad (3)$$

While only considering steady friction is sufficient to estimate the initial magnitude of a pressure transient in the system, an additional unsteady friction term will improve the simulated dissipation of such a pressure wave over time (Chaudhry 2014). The equations resulting from these changes and adapted to represent flow rates rather than fluid velocities are shown in Eq. 4 and Eq. 5.

$$\frac{\partial H}{\partial t} = -\frac{a^2}{gA} \frac{\partial Q}{\partial x} \quad (4)$$

$$\frac{\partial Q}{\partial t} = -gA \frac{\partial H}{\partial x} - S_s - S_u \quad (5)$$

The additional  $Q$ ,  $A$ ,  $S_s$  and  $S_u$  are volumetric flow rate, cross-sectional area of the conduit, steady and unsteady friction losses. The steady friction losses can be calculated using the Darcy-Weisbach formulations using the friction factor  $f$  as shown in Eq. 6 (Riasi et al. 2010). For the unsteady friction losses, a one-coefficient model,  $k$ , of an instantaneous acceleration-based method is used as shown in Eq. 7 (Chaudhry 2014). The fluid accelerations that induce these losses, are calculated from the averaged cross-sectional values. With values between 0.015 and 0.06 m/s<sup>2</sup> the coefficient  $k$  has been shown to closely match experimental results.

$$S_s = \frac{fQ|Q|}{2DA} \quad (6)$$

$$S_u = \frac{k}{g} \left[ \frac{\partial Q}{\partial t} + \text{Sign}(Q)a \left| \frac{\partial Q}{\partial x} \right| \right] \quad (7)$$

To solve the conduit equations, the partial differential equations are transformed to ordinary differential equations using a central scribed finite difference method. In order to accurately simulate hydraulic transients within the system, the states of pressure and flow rates should be known across the whole space and time. Practically, the spatial dimension is discretised and the temporal steps solved via a numerical integration scheme. Results are obtained simultaneously along the spatial dimension and consecutively for the temporal steps. The resulting grid of nodes is illustrated in figure 1. The temporal increments are indicated by the subscript  $i$  and the spatial by  $j$ .

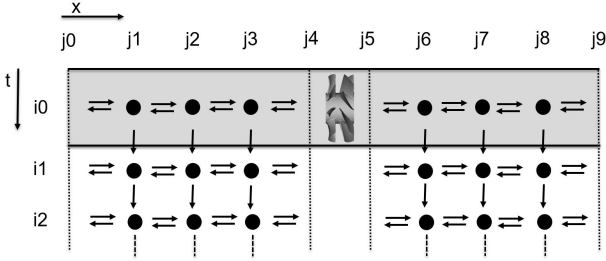


Figure 1: Node grid used for spatial and temporal discretization.

Using the central finite difference method the  $\frac{\partial Q_{i,j}}{\partial x}$  and  $\frac{\partial H_{i,j}}{\partial x}$  terms can now be replaced by  $\frac{Q_{i,j+1} - Q_{i,j-1}}{2\Delta x}$  and  $\frac{H_{i,j+1} - H_{i,j-1}}{2\Delta x}$  with  $\Delta x$  referring to the spatial distance between nodes. The finite difference method is chosen due to its simplicity and ease of implementation when applied to sets of coupled equation with one of the disadvantages being the requirement of a regular node grid (Benito et al. 2001).

## 2.2 Boundary conditions

To solve for the transient-state pressure head and flow rate at the boundaries of the conduit and to the two contra-rotating runners, Eq. 4 and Eq. 5 need to be simultaneously solved with the boundary conditions imposed. To develop these boundary conditions, the method of characteristics is used resulting in algebraic equations describing the relationship between pressure head and flow rate. The basic characteristic equations for upstream and downstream boundaries as described by Chaudhry (2014) are shown in Eq. 8 and Eq. 9.

$$Q_{i,j} = Q_{i,j+1} - \frac{gA}{a} H_{i,j+1} - \frac{f}{2DA} \Delta t Q_{i,j+1} |Q_{i,j+1}| + \frac{gA}{a} H_{i,j} \quad (8)$$

$$Q_{i,j} = Q_{i,j-1} + \frac{gA}{a} H_{i,j-1} - \frac{f}{2DA} \Delta t Q_{i,j-1} |Q_{i,j-1}| - \frac{gA}{a} H_{i,j} \quad (9)$$

If the upstream and downstream boundaries represent the connection to a reservoir, the entrance losses can be accounted for using Eq. 10 and Eq. 11. Here  $h_e$  are the entrance head losses to the conduit,  $k_e$  is the entrance loss coefficient and  $H_{res}$  the total head at the reservoir.

$$h_e = \frac{k_e Q_{i,j}^2}{2gA_j^2} \quad (10)$$

$$H_{i,j} = H_{res} - h_e \quad (11)$$

If the reservoir is assumed to be large enough that travelling pressure waves would be entirely absorbed, non-reflecting boundaries can be implemented. To do so, the terms accounting for the pressure difference between the boundary and the neighbouring node are removed. In a friction-less system this leaves the boundary flow rate to be equal to the flow rate at the neighbouring node.

If characteristic equations are used, the spatial and temporal steps have to be chosen correctly to ensure a stable solution and hence accurately represent a pressure wave propagating through the conduit. Neglecting non-linear terms the Courant condition shown in Eq. 12 can be used to determine the appropriate spatial distance between nodes for a given time step or vice versa (Ghidaoui et al. 2005). E.g. assuming a maximum wave velocity of 1480 m/s combined with a spatial distance between nodes of 0.148 m would result in 0.1 ms timesteps. To reach a sufficient level of accuracy a minimum node density is required. In an iterative process the spatial distance can be reduced until no further improvements are achieved.

$$\Delta x \geq a \Delta t \quad (12)$$

To fully develop the boundaries at the turbine as well as to couple the conduit model to the other sub-models, characterising the hydrodynamic performance of the rotors is required.

## 2.3 Coupling to drivetrain and motor-generators

A variable speed power take-off is chosen due to its improved flexibility and efficiencies across a wider range of operating conditions (Vasudevan et al. 2021). The proposed system uses direct-drive transmissions

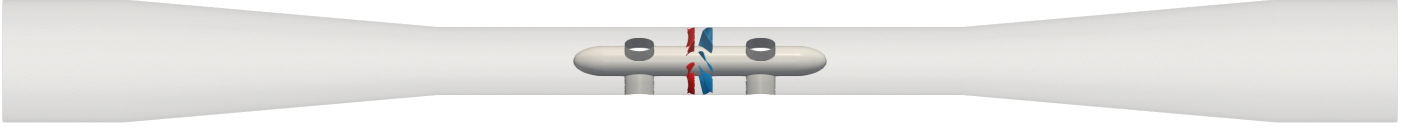


Figure 2: Modelling Domain for CFD comparison, including hub, struts and runners. (Fahlbeck et al. 2022b)

coupling the two runners to their individual motor-generators. Neglecting flexibility in the drivetrain components, the angular velocities can be assumed constant along the driveshaft between runners and motor-generators. This allows to model each drivetrain as an individual rigid body with an equivalent rotational inertia to account for the different rotating parts leading to Eq. (13) and Eq. (14) (Leithead and Connor 2000).

$$J_1 \frac{d\omega_1}{dt} = \tau_{h1} - \tau_{g1} - D_{f1}\omega_1 \quad (13)$$

$$J_2 \frac{d\omega_2}{dt} = \tau_{h2} - \tau_{g2} - D_{f2}\omega_2 \quad (14)$$

Here we have  $J_{1,2}$  as the rotational inertias,  $\omega_{1,2}$  as the angular velocities,  $\tau_{h1,2}$  as hydraulic torques,  $\tau_{g1,2}$  as generator torques and  $D_{f1,2}$  as a viscous damping torque coefficient to account for torque losses. The conduit model is coupled to both of these drivetrains via the hydraulic torques determined by flow rate, pressure drop across the individual runners  $h_{1,2}$ , runner efficiencies  $\eta_{1,2}$ , fluid density  $\rho$  and their respective angular velocities as shown in Eq. (15).

In return the angular velocities of both runners combined with the flow rate determine the pressure drop across them as well as their efficiencies illustrated in Eq. (16) and Eq. (17). This relationship is determined through the aforementioned characterisation of the runners. Such a characterisation can be based on a range of CFD simulations or experimental results of the particular rotor design under steady-state conditions. By doing a multi-variant regression on such data, the pressure drop across, as well as the efficiency of both rotors, can be expressed as a function of flow rate and both angular velocities.

$$\tau_{h1,2} = \frac{\rho g Q h_{1,2} \eta_{1,2}}{\omega_{1,2}} \quad (15)$$

$$h_{1,2} = f(Q, \omega_1, \omega_2) \quad (16)$$

$$\eta_{1,2} = f(Q, \omega_1, \omega_2) \quad (17)$$

The governor controlling the angular velocities of the runners is coupled through the generator torques. If an additional control variable is required, a valve that is able to regulate the flow from the conduits to the runners can be added to the system.

### 3 RESULTS

Following, the results of two scenarios, applied to the model outlined in the previous section, are presented. The methodology and setup are explained before the sensitivity using varying node densities for the finite difference method are compared. Lastly the results are compared to CFD simulations.

#### 3.1 Methodology & system properties

The setup and initial conditions for the results used for comparing the model and CFD simulations are based on a scaled down version of the system with a runner diameter of 27.6 cm. On both sides of the pump-turbines, draft tubes increase the pipe diameter to 50 cm connecting the upper and lower reservoir. The static head difference between these reservoirs is 6.45 m. Since the model results are compared with the results of CFD simulations done by Fahlbeck et al. (2022b), the same domain is used for the numerical model. This domain is shown in figure 2.

Aside from the initial conditions of pressure and flow rate across the conduit, the main input to the model are the static heads at the upper and lower reservoir. These are based on the static head difference expected in the lab. Major and minor head losses outside of the domain are included. These consist of entrance and exit losses from the lower and upper reservoir, a pipe bend, a fixed and a variable valve. For both scenarios the fixed and variable valve are considered fully open. Additionally the major losses for an additional 1 m of pipe upstream of the pump-turbine and 15.5 m downstream of it are applied. Coefficients are chosen to match the CFD simulations. The parameters used for the simulations are shown in table 1.

Table 1: Model parameters used for the simulations.

Static head upper reservoir	$H_{ures}$	9.7	m
Static head lower reservoir	$H_{lres}$	3.25	m
Pressure wave velocity	$a$	1200	m/s
Surface roughness	$e$	0.05	mm
Unsteady loss coefficient	$k$	0.04	m/s <sup>2</sup>
<b>Minor loss coefficients</b>			
Entrance		0.45	-
Exit		1	-
Bend		0.2	-
Fixed Valve (fully open)		0.4	-
Variable Valve (fully open)		0.39	-

To compare the model against the CFD results and ensure that no tuning of parameters is required for individual cases to match, two scenarios are analysed. Between these cases no changes are made to the

model setup. The first is a start-up sequence and the second a change of operating point. The CFD simulations were done with both a high- and low-fidelity model with one order of magnitude difference in number of mesh cells. The comparison is based on the results of the high-fidelity model. The methodology and boundaries used for the CFD simulations are described in further detail by Fahlbeck et al. (2021) and Fahlbeck et al. (2022a).

### 3.2 Start-up sequence

To start up the system in pump mode, the chosen case accelerates the runners from an initial 916 RPM to their final operating point at 1502 RPM over a period of 3 s. At this initial angular velocity the net head produced by the pump-turbine matches the gross head of the system resulting in zero flow. The angular velocity of the two runners for the sequence is shown in figure 3.

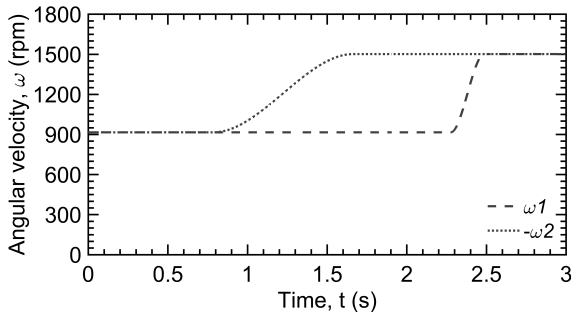


Figure 3: Angular velocity during start-up.

To determine the required node density, this sequence is first simulated with 20, 40 and 60 nodes. The resulting conduit flow rate for modelling the system with these varying node densities can be found in figure 4. There is no relevant difference between the 40 and 60 node model. When reduced to 20 nodes, minor differences in the dynamics are noticeable. However, in steady state all solutions converge. The 20 node model takes about 28 % of the computational time to solve compared to the 60 node model. For all further results the 40 node model is used. This results in a spatial distance between nodes of around 13.3 cm. Together with a pressure wave velocity of 1200 m/s the simulation time step is chosen at about  $1.1 \times 10^{-4}$  s.

The comparison of flow rates during the start-up sequence between the 40 node model and CFD results is shown in figure 5. At the final operating points the results are closely matched with a difference of only 1.3 %. However, the flow rate of the CFD simulation is slightly more stable in steady state. At the initial acceleration of runner two and the consequent increase in pump head over the RPT, the flow rate in the proposed model reacts slower compared to the CFD results. This marginally slower reaction time to changes in the pump head is also visible after runner

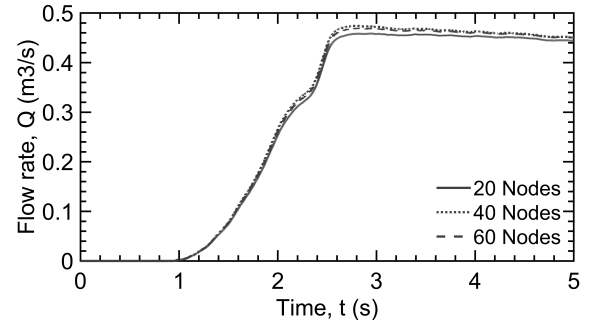


Figure 4: Flow rate for varying node density.

two reaches its final angular velocity and before runner one is accelerated. After the acceleration of runner one, the flow rate of the model overshoots before converging.

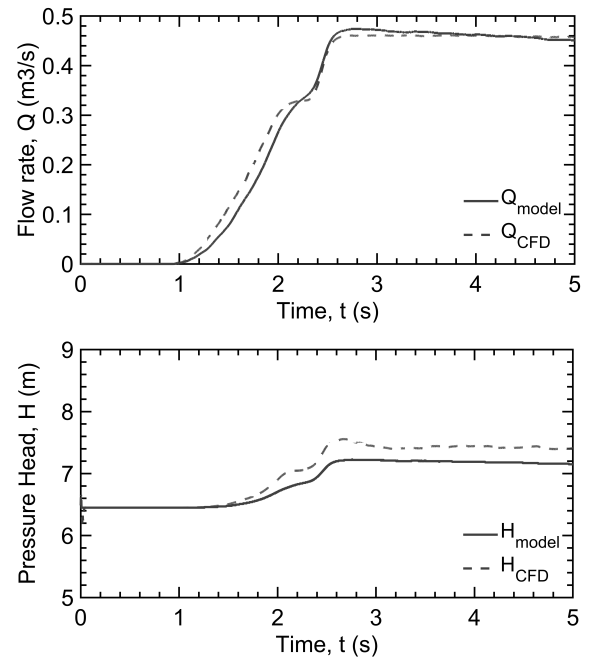


Figure 5: Flow rate and pressure head over the computational domain of model and CFD simulation - start up sequence.

The pressure head over the domain is shown in the same figure. The head in the CFD results clearly rises faster, reaches a higher maximum during the acceleration of runner one and remains higher in steady state. At the final operating point the head over the CFD domain reaches around 7.4 m compared to 7.16 m over the proposed model. This reflects a 3.4 % difference.

Since the final flow rates and the static heads are similar for both results, the overall losses should be roughly equivalent. However, the reduced head over the model domain indicates that the losses outside of the domain are slightly lower compared to the CFD and the losses within the domain slightly higher. The slower response of the model flow rate to changes in pump head could also be caused by these higher steady or unsteady losses within the domain. Inaccuracies may be introduced through the use of equivalent friction factors and cross-sections along the conduit as well as the use of a static pressure wave velocity.

### 3.3 Change of operating point

To ensure consistent and repeatable modelling results for varying scenarios and operating conditions, a second case is compared. This second case simulates a rapid change between operating points. This particular scenario starts at the final operating point of the start-up sequence, before reducing the angular velocity of runner two down to 1129 RPM as shown in figure 6. This corresponds with a sudden reduction in power by about 22 % over a period of 1 s.

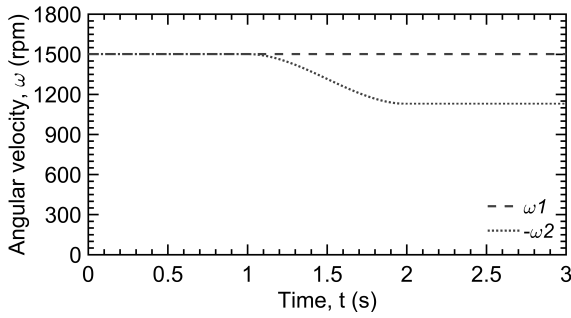


Figure 6: Angular velocity during change of operating point.

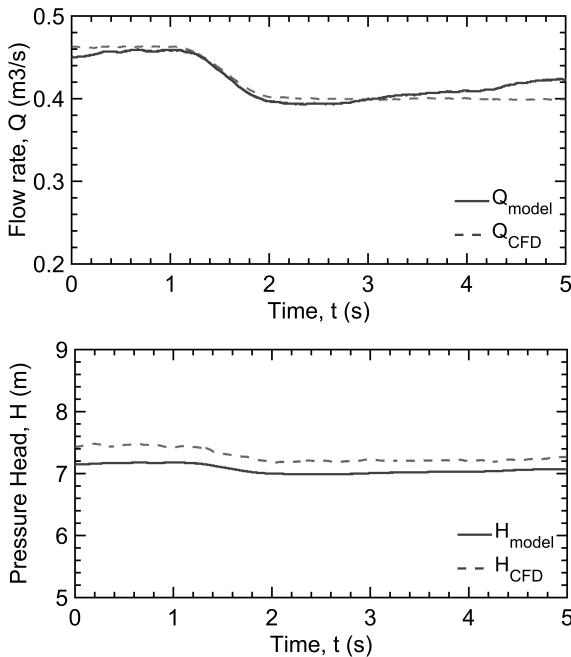


Figure 7: Flow rate and pressure head over the computational domain of model and CFD simulation - change of operating point.

The resulting flow rate and pressure head over the domain from the model and CFD simulation can be found in figure 7. The flow rate in the model starts at a lower operating point and overshoots after the decrease in angular velocity of runner two and the corresponding reduction in pump head. It reacts marginally faster than in the CFD results. This further supports the conclusion drawn from the first case that the difference in dynamic reaction may be caused by slightly overestimated losses within the domain. Aligned with the first case the pressure head over the domain is about 2.6 % higher in the CFD results.

After runner two reaches the final operating point, the flow rate of the CFD simulation stabilises while the flow rate in the model keeps increasing resulting in a difference of about 6.2 % at the final operating point. Such a divergence over time is most probably caused by changes in the pump head. Since the head is determined through the runner characterisation, the inaccuracy in the model is likely introduced by a mismatch between characterisation and actual pump head.

## 4 CONCLUSIONS

A system model to investigate the dynamics and component interaction of a low-head pumped hydro storage plant has been proposed. While using the model compared to CFD simulations can decrease significantly the required computational resources, a compromise in the results accuracy is expected. One of the major differences is that the model is based on a one dimensional approach. This means that velocity and pressure values are averaged in the cross-sections perpendicular to the flow. Consequently, localised pressure variations are not covered which are crucial when predicting effects such as cavitation. Additionally non-axial fluid velocities are not included potentially leading to inaccurate loss approximations.

The comparison of the model results using varying node densities has shown that, for the setup used in the simulations, no further improvements to accuracy can be achieved beyond 40 nodes and the consequent spatial distance of around 13.3 cm. The comparison of the results to CFD simulations demonstrated that a simplified one dimensional model can produce satisfactory results covering the relevant dynamics of the system. In steady state the resulting flow rates and pressure heads of the model are within a small deviation of the CFD results.

While there can be improvements made to better cover the losses within the conduit and the runner characterisation, overall the results between the proposed model and CFD simulations are closely matched. This enables the more efficient model to be used to investigate system dynamics for varying components and operating conditions. To further verify the results an experimental validation should be conducted.

## ACKNOWLEDGEMENTS

This research is part of a project that has received funding from the European Union's Horizon 2020 research and innovation programme under grant agreement No. 883553.

## REFERENCES

Adamkowski, A. (2003). Analysis of transient flow in pipes with expanding or contracting sections. *Journal of Fluids Engi-*



- neering, *Transactions of the ASME* 125(4), 716–722.
- Benito, J. J., F. Ureña, & L. Gavete (2001, 12). Influence of several factors in the generalized finite difference method. *Applied Mathematical Modelling* 25(12), 1039–1053.
- Chaudhry, M. H. (2014). *Applied hydraulic transients*.
- Fahlbeck, J., H. Nilsson, & S. Salehi (2021). Flow Characteristics of Preliminary Shutdown and Startup Sequences for a Model Counter-Rotating Pump-Turbine. *Energies* 14(12), 3593.
- Fahlbeck, J., H. Nilsson, & S. Salehi (2022a, 1). A Head Loss Pressure Boundary Condition for Hydraulic Systems. *Open-FOAM Journal* 2, 1–12.
- Fahlbeck, J., H. Nilsson, & S. Salehi (2022b). Evaluation of startup time for a model contra-rotating pump-turbine in pump-mode. *IOP Conference Series: Earth and Environmental Science*.
- Ghidaoui, M. S. (2004, 6). On the fundamental equations of water hammer. *Urban Water Journal* 1(2), 71–83.
- Ghidaoui, M. S., M. Zhao, D. A. McInnis, & D. H. Axworthy (2005, 1). A Review of Water Hammer Theory and Practice. *Applied Mechanics Reviews* 58(1), 49–76.
- Hoffstaedt, J. P., D. P. Truijen, J. Fahlbeck, L. H. Gans, M. Qudaih, A. J. Laguna, J. D. De Kooning, K. Stockman, H. Nilsson, P. T. Storli, B. Engel, M. Marence, & J. D. Bricker (2022, 4). Low-head pumped hydro storage: A review of applicable technologies for design, grid integration, control and modelling. *Renewable and Sustainable Energy Reviews* 158.
- Leithead, W. E. & B. Connor (2000). Control of variable speed wind turbines: Dynamic models. *International Journal of Control* 73(13), 1173–1188.
- Mohanpurkar, M., A. Ouroua, R. Hovsapian, Y. Luo, M. Singh, E. Muljadi, V. Gevorgian, & P. Donalek (2018). Real-time co-simulation of adjustable-speed pumped storage hydro for transient stability analysis. *Electric Power Systems Research* 154, 276–286.
- Qudaih, M., B. Engel, D. Truijen, J. De Kooning, K. Stockman, J. Hoffstädt, A. Jarquin-Laguna, R. Ansorena Ruiz, N. Goseberg, J. Bricker, J. Fahlbeck, H. Nilsson, L. Bossi, M. Joseph, & M. Zangeneh (2020). The contribution of low-head pumped hydro storage to a successful energy transition. In *Proceedings of the Virtual 19th Wind Integration Workshop*, pp. 8.
- REN21 (2021). *Renewables 2021 Global Status Report*.
- Riasi, A., M. Raisee Dehkordi, & A. Nourbakhsh (2010, 06). Simulation of transient flow in hydroelectric power plants using unsteady friction. *Strojniski Vestnik* 56.
- Sharma, J. D. & A. Kumar (2014). Development and Implementation of Non-Linear Hydro Turbine Model with Elastic Effect of Water Column and Surge Tank. *International Journal of Electrical and Electronics Research* 2(4), 234–243.
- Stecki, J. S. & D. C. Davis (1986). Fluid transmission lines-distributed parameter models Part 1: a review of the state of the art. *Proc. Inst. Mech. Engrs. Part a* 200(A4, 1986), 215–228.
- Vasudevan, K. R., V. K. Ramachandaramurthy, G. Venugopal, J. B. Ekanayake, & S. K. Tiong (2021). Variable speed pumped hydro storage: A review of converters, controls and energy management strategies. *Renewable and Sustainable Energy Reviews* 135, 110156.